ZAMM · Z. Angew. Math. Mech. **92**, No. 1, 41 – 51 (2012) / **DOI** 10.1002/zamm.201000210

Interface delamination of bi-material structure under time harmonic load. Cohesive behaviour of the interface

Jordanka Ivanova[1,*], **Gergana Nikolova**[1,**], **and Barbara Gambin**[2,***]

[1] Institute of Mechanics, BAS, Akad. G. Bonchev Str., bl. 4, 1113 Sofia, Bulgaria
[2] Institute of Fundamental Technological Research, Pawinskiego Str. 5 b, 02-106 Warsaw, Poland

Received 19 November 2010, revised 9 February 2011, accepted 28 May 2011
Published online 5 August 2011

Key words Dynamic behaviour of bi-material structure, cracked plate, shear lag model, Laplace transform, cohesive interface delamination, cohesive debond length.

The interface cohesive behaviour and interface delamination in a bi-material structure consisting of two plates and material interface with zero thickness under time harmonic load is studied. Previously, the authors studied the elasto-brittle interface behaviour, from both sides of a crack, initially normal to the interface, when the elastic-brittle interface debonding appeared. Now, it is again assumed that the restriction for the ratio of energy release rates of the second plate and interface allowing the occurrence of an interface cohesive delamination before the initiation of the normal crack in the second plate is satisfied. The shear lag model is adopted and applied to find the dynamic response of the considered structure, assuming the cohesive interface behaviour, accompanied before of the elastic-brittle one. In both cases, the growth of debond length is not considered e.g. at a given loading condition the corresponding single debond length is found. The inertia forces of the already debonded interface elasto-brittle cracks (mode II) are neglected. The appropriate contact conditions are proposed in order to fit together both elastic and cohesive solutions. The Laplace inverse transform is applied to obtain the original of cohesive debond length by the aid of the already obtained elastic value of debond length at the same loading condition. Parametric analysis of the results obtained is illustrated by examples of the modern ceramic-metal composite on metal substrate. The influence of frequencies and amplitude fluctuations on the cohesive debond length and the interface shear stress distribution are discussed.

1 Introduction

The shear lag approach is one of the most used analytical tools in mechanics of composite materials. The paper of Dowling and Burgan [1] as well as the paper of Cox [2] traces the interest in shear lag of aircraft and ship design from the early days to the more recent attention devoted to it by structural engineers. The main idea of the shear-lag analysis is such an assumption which involves a simplification of in-plane shear stress τ_{xy} and decouples the 2D problem into two 1D ones. Hedgepeth [3] was the first who applied shear-lag model to unidirectional composites. The shear lag model has been adopted and successfully used by many authors, e.g. [4–16]. Ivanova at al. [13–16] applied the shear lag approach to the bi-material layered structure with pre-cracked first layer. Different loadings are considered: static, thermal, and combined thermo-mechanical ones. The elastic-brittle, sleep, and cohesive behaviour of the interface was assumed and the respective debond length is found. The comparison between shear lag prediction [15,16] with Song's experimental data for the elastic-brittle debond length for bi-material structure Zinc/Steel as well as with respective result from FEM simulation 17 shows a good agreement.

The shear lag approach is also intensively used in the interface fracture mechanics considering the cracking, decohesion and delamination of thin film on a substrate. A very important (basic) case in the fracture mechanics of thin films is the problem of an elastic thin film with a vertical crack, the tip of which touches or is at some distance from the interface, investigated by Beuth in [18]. The mechanisms and fracture characteristics of cracks in a film on a substrate were analyzed also by Hutchinson and Suo [19]. Plastic yielding of the substrate and film was accompanied: by the vertical cracking in the films and the interface fracture [18, 19], delamination from the ends of the vertical crack in the film [20], crack extension in the substrate along the interface [21], multiple interface cracks [22], etc. For woven fabric and hybrid composites, the dynamic bond stress in bi-material elastic homogeneous semi-infinite layers subjected to a pressure load steps along the end surfaces was studied in [23, 24], but the delamination along the interface was not studied. By using the technique of

* E-mail: ivanova@imbm.bas.bg
** E-mail: gery@imbm.bas.bg
*** Corresponding author E-mail: Barbara.Gambin@ippt.gov.pl

Laplace transforms, closed form solutions of the dynamic displacements and stresses in each yarn, the shearing stresses at the interfaces between adjacent yarns, were obtained in the transformed domain. The results for a step uniform impact are presented as an example. In [25] the beam theory is used to study dynamic mode I crack propagation through-thickness reinforced laminar structures loaded with a flying wedge. Although well known advantages of the shear lag method, its usage and applicability in the field of dynamics is still insufficient.

The origins of the concept of the cohesive zone model goes back to work of Barenblatt [26] and Dugdale [27], where the model has been involved as a preferred method to analyze fracture behaviour in monolithic and composite materials. All other models implemented in metallic and ceramic materials, reinforced polymer composites, and bi-material structures start from the assumption that at least one interface can be defined where crack propagation is allowed by the introduction of a possible discontinuity in the displacement field. Various interface cohesive laws were proposed (Hilleborg et al. [28], Rose et al. [29], Needleman [30], Tvergaard [31], Tvergaard and Hutchinson [32], Xu and Needleman [33]). The main difference between these laws lies in the shape of the traction-displacement response.

The objective of this work is to continue investigations on the dynamic cohesive behaviour, accompanied with elastic brittle one for a bi-material pre-cracked structure under a given sinusoidal dynamic load. The method used in [34], e.g. the shear lag combined with the Laplace transform will be also applied. The considered 2D structure is modeled as two different adjacent material plates, namely A and B, with prescribed properties.

In order to activate the mechanism depicted in Fig. 1 (Sect. 2), it is essential that the initial mode I crack when it reaches the interface does not penetrate the second plate, but rather kinks along the interface and give an interfacial elastic-brittle delamination.

A restriction for the ratio of energy release rates of plates, which allows occurring of the interface delamination first and before the initiation of the normal crack in the second plate is needed. It is assumed that the ratio of energy release rates of plates, which allows occurring of the interface delamination first and before the initiation of the normal crack in the second plate has to be satisfied.

To the knowledge of the authors, no investigations by shear lag analysis are known until now for the subject of the interface cohesive delamination (decohesion), accompanied by an elasto-brittle one in bi-material structures subjected to dynamic time-harmonic loads, despite the fact that a variety of static analysis of different kinds of composites has been performed.

Further the authors will name the result of the interface decohesion as cohesive single debond length.

In the present paper both shear lag analysis and Laplace transform are used to obtain the cohesive single debond length along the interface. The value of the cohesive debond length is determined through suitable contact conditions for fitting together the elastic [34] and cohesive solutions. The growth of debond length is not considered. All results obtained as well as the parametric analysis of the results obtained are illustrated by figures and discussed.

2 Analytical model

Following [34] it is assumed that the periodic bi-material structure consists of a two elastic plates with different material properties and material interface. The bi-material structure begins with harder material (ceramics), interface and softer material. The first plate A is pre-cracked by a transient crack (mode I), reaching the interface. In the previous paper [34], due to the assumed elastic brittle interface behaviour, the interface delaminates from both sides of a normal crack with a

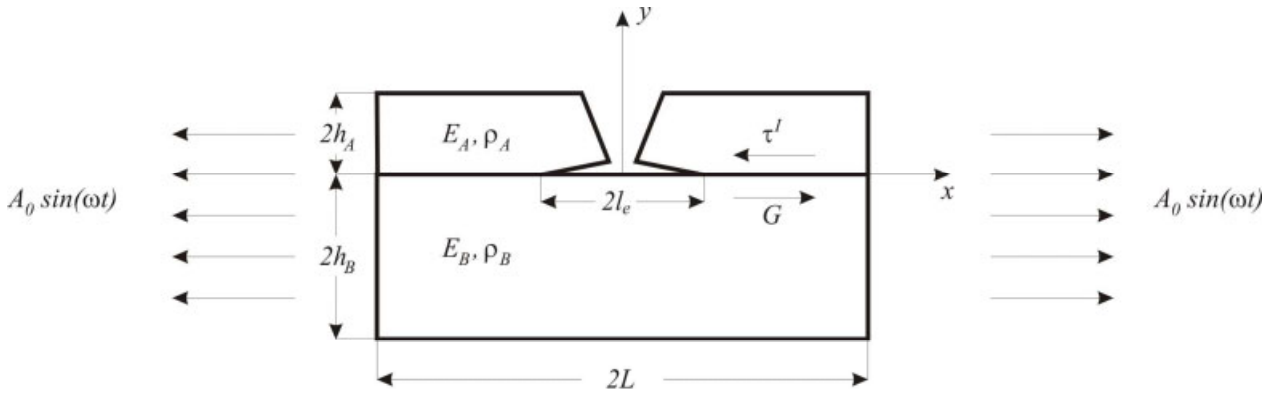

Fig. 1 Bi-material structure under time-harmonic dynamic excitation.

single elatic-brittle debond length (mode II). The restriction on the ratio of energy release rates is assumed to satisfy the arising of interface delamination before the condition for arising the normal crack in the plate B.

Every plate has Young modulus$E$, mass densityρ, thickness$h$, axial displacement $u(x,t)$ and axial stress $\sigma(x,t)$, where t, x denote time and axial coordinate, respectively. The total length of the cell is $2L$. The structure is exited again by a dynamic load $A_0 \sin(\omega t)$ over the ends $x = \pm L$, see Fig. 1. The inertia forces of the already debonded parts with length l_e of the plates A and B are not taken into account.

The material interface I is supposed to be with a zero thickness and working only on shear with a shear modulus G, a shear stress $\tau^I(x,t)$, where a superscript I for shear stress τ^I and displacement $u^I = u_A - u_B$ belongs to the interface. The plates are modeled as isotropic elastic materials, while the cohesive law governs the interface behaviour.

The axial stresses and strains are uniform over the cross section of each plate, working only on tension-pressure. The bending is neglected.

The goal of this study is to determine the dynamic response of the bi-material structure, having mode II elastic-brittle crack along the interface with length l_e as well as to predict the next single debond cohesive length along the interface (see Fig. 1).

3 Cohesive behaviour of the interface

The behaviour of the interface shear stress τ^I as a function of interface displacement u_I^c is assumed as cohesive one (see Fig. 2).

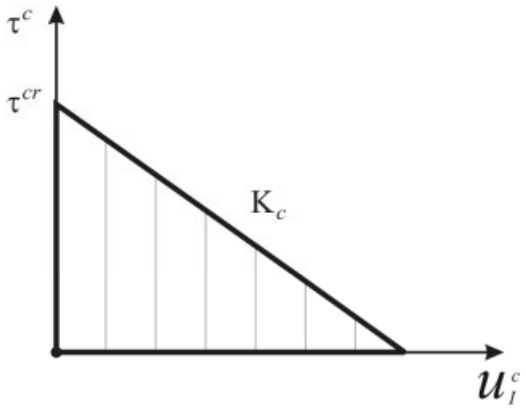

Fig. 2 The diagram τ^c–u_I^c.

Following the assumption of the shear lag model, the governing dynamic Eqs. (1), constitutive equations (2), initial (3) and boundary conditions (4) are proposed, respectively as

$$\begin{aligned} E_A \frac{\partial^2 u_A^c}{\partial x^2} - \frac{\tau^I}{2h_A} &= \rho_A \frac{\partial^2 u_A^c}{\partial t^2}, \\ E_B \frac{\partial^2 u_B^c}{\partial x^2} + \frac{\tau^I}{2h_A} &= \rho_B \frac{\partial^2 u_B^c}{\partial t^2}, \end{aligned} \tag{1}$$

$$\begin{aligned} &\tau^I = \tau^c = \tau^{cr} - K_c \frac{u_A^c - u_B^c}{h_A + h_B}, \quad u_I^c = \frac{u_A^c - u_B^c}{h_A + h_B}, \\ &\sigma_A(x,t) = E_A \frac{\partial u_A^c}{\partial x}, \quad \sigma_B(x,t) = E_B \frac{\partial u_B^c}{\partial x}, \end{aligned} \tag{2}$$

$$u_A^c(x,0) = u_B^c(x,0) = 0, \quad \left.\frac{\partial u_A^c(x,t)}{\partial t}\right|_{t=0} = \left.\frac{\partial u_B^c(x,t)}{\partial t}\right|_{t=0} = 0, \tag{3}$$

$$\begin{aligned} \sigma_A^c(x,t)|_{x=L} &= A_0 \sin(\omega t), \\ \sigma_B^c(x,t)|_{x=L} &= A_0 \sin(\omega t), \end{aligned} \tag{4}$$

where by $u_i^c,\ E_i,\ \rho_i,\ h_i,\ \sigma_i^c; i = A, B$ the displacements, Young moduli, densities, thicknesses, and stresses of the plates are denoted, respectively. By $\tau^I,\ \tau^{cr},\ K_c, u_I^c$ the interface shear stress, its critical value, the cohesive softening modulus,

and interface displacement are denoted, respectively. Note that in (1) the continuity conditions for the equality of elastic (u_i^e) and cohesive (u_i^c) displacements and their respective derivatives $u_i'^{e,\,c}$ at the point $X = l_e$ are taken into account.

Subscripts $A,\ B$ denote material and geometric parameters of plates. By superscripts "$c,\ e$" the respective cohesive or elastic displacements, stresses, and strains are denoted.

According to [34], the following non-dimensional parameters $\bar{u}_i^c, \bar{L}, \bar{\tau}^c, \bar{\sigma}_i^c, \bar{l}_i, \xi, \eta$ are introduced

$$
\begin{aligned}
&u_{_i}^c = (h_A + h_B)\bar{u}_{_i}^c, \quad L = \alpha\bar{L}, \quad \tau^c = C\bar{\tau}^c = G(\bar{\tau}^{cr} - \bar{K}_c(\bar{u}_A^c - u_B^c)), \quad K_c = G\bar{K}_c,\\
&\sigma_i^c = E_A\bar{\sigma}_i^c, \quad i = A, B\\
&x = \alpha\xi, \quad \alpha = \left[\frac{2h_AE_A}{G}(h_A + h_B)\right]^{1/2}, \quad l_j = \alpha\,\bar{l}_j, \quad j = e, c\,,\\
&t = \beta\eta, \quad \beta = \left[\frac{2h_A\rho_A}{G}(h_A + h_B)\right]^{1/2}, \quad \eta_1 = \frac{E_A}{E_B}, \quad \mu = \frac{\rho_A}{\rho_B}, \quad \varsigma = \frac{h_A}{h_B}.
\end{aligned}
\tag{5}
$$

Eqs. (1) become

$$
\begin{aligned}
&\frac{\partial^2\bar{u}_A^c}{\partial\xi^2} + \bar{K}_c(\bar{u}_A^c - \bar{u}_B^c) = \frac{\partial^2\bar{u}_A^c}{\partial\eta^2} + \bar{\tau}^{cr},\\
&\frac{\partial^2\bar{u}_B^c}{\partial\xi^2} - \lambda^2\bar{K}_c(\bar{u}_A^c - \bar{u}_B^c) = c^2\frac{\partial^2\bar{u}_A^c}{\partial\eta^2} - \lambda^2\bar{\tau}^{cr},
\end{aligned}
\tag{6}
$$

where $\lambda^2 = \varsigma\eta_1$, $c^2 = \frac{\eta_1}{\mu}$.

Further the lines over $\bar{u}_{A,B},\ \bar{L},\ \bar{\tau}^I,\ \bar{\sigma}_{A,B},\ \bar{l}_j$ are omitted, but remembered.

The initial and boundary conditions become

$$
\begin{aligned}
&u_A^c(\xi, 0) = u_B^c(\xi, 0) = 0, \quad \left.\frac{\partial u_A^c}{\partial\eta}\right|_{\eta=0} = \left.\frac{\partial u_B^c}{\partial\eta}\right|_{\eta=0} = 0,\\
&\sigma_A^c(\xi,\eta)|_{\xi=L} = \frac{\partial u_A^c}{\partial\xi} = B_0\sin(\omega\eta), \quad B_0 = A_0a_0/(E_AG)^{1/2}, \quad a_0 = \left[\frac{2h_A}{(h_A + h_B)}\right]^{1/2},\\
&\sigma_B^c(\xi,\eta)|_{\xi=L} = \frac{\partial u_B^c}{\partial\xi} = \eta_1B_0\sin(\omega\eta) \quad \text{for every } \eta.
\end{aligned}
\tag{7}
$$

To solve the problem, given by Eqs. (6)–(7), the Laplace transform will be used. The following procedure for finding the analytical solution of Eqs. (6) together with (7) is proposed.

Let us introduce the one side Laplace transform pairs $\tilde{f},\ f$ (the Laplace image and original functions, respectively) as follows

$$
\tilde{f}(\xi, s) = \int_0^\infty f(\xi,\eta)\exp(-s\eta)d\eta \quad \text{and } f(\xi,\eta) = \tfrac{1}{2\pi i}\lim_{T\to\infty}\int_{\gamma-iT}^{\gamma+iT} f(\xi, s)\exp(s\eta)ds,
$$

where γ is a real number. The contour path of integration is in the region of convergence of $\tilde{f}(\xi, s)$, requiring $\gamma > \mathrm{Re}(s_p)$ for every singularity s_p of $\tilde{f}(\xi, s)$. If $\mathrm{Re}(s_p) < 0$ for every s_p, then $\gamma = 0$ and the inverse integral formula becomes identical to the inverse Fourier transform.

Applying Laplace transform to Eqs. (6) we obtain

$$
\begin{aligned}
&\frac{d^2\tilde{u}_{_A}^c}{d\xi^2} + K_c(\tilde{u}_{_A}^c - \tilde{u}_{_B}^c) = s^2\tilde{u}_{_A}^c + \frac{\tau^{cr}}{s},\\
&\frac{d^2\tilde{u}_{_B}^c}{d\xi^2} - \lambda^2K_c(\tilde{u}_{_A}^c - \tilde{u}_{_B}^c) = s^2c^2\tilde{u}_{_B}^c - \frac{\lambda^2\tau^{cr}}{s}.
\end{aligned}
\tag{8}
$$

Further the tilde over $\tilde{u}_{A,B}$ is omitted, but remembered. From (8/1) we have

$$
u_{_B}^c = \frac{1}{K_c}\left(\frac{d^2u_{_A}^c}{d\xi^2} + \left(K_c - s^2\right)u_{_A}^c - \frac{\tau^{cr}}{s}\right).
$$

Replacing this relation in (8/2) the following governing ordinary differential equation about u_A^c is obtained

$$\frac{d^4u_A^c}{d\xi^4} + U(s)\frac{d^2u_A^c}{d\xi^2} + T(s)u_A^c - Y(s) = 0, \tag{9}$$

where $T(s) = s^2[c^2s^2 - K_c\left(\lambda^2 + c^2\right)]$, $\quad U(s) = K_c(1+\lambda^2) - s^2(1+c^2)$, and $Y(s) = -s^2c^2\tau^{cr}$.

Eq. (9) has to be solved with boundary and contact conditions given by (10). The contact conditions are the result of the fitting together both elastic [34] and cohesive solutions and consist in equalities of elastic and cohesive displacements and their first derivatives. The contact conditions are posed at the point of translation $\xi' = \xi - l_e$ of the initial origin of the Cartesian coordinate system (see Fig. 1) of the axes 0ξ for elastic solution [34]. Then the obtained elastic solution is in the interval $\xi' = [0,\ (l - l_e)]$, while the cohesive solution starts from $\xi = l_e$ and is determined in the interval $\xi = [0,\ l_e]$.

$$\begin{aligned}
&u_A^c(l_e) = u_A^e(0) = \frac{\tau^{cr}}{s},\\
&u_B^c(l_e) = u_B^e(0) = 0,\\
&\left.\frac{du_A^c}{d\xi}\right|_{(l_e,s)} = \left.\frac{du_A^e}{d\xi}\right|_{(0,s)} = 0,\\
&\left.\frac{du_B^c}{d\xi}\right|_{(l_e,s)} = \left.\frac{du_B^e}{d\xi}\right|_{(0,s)} = r_1r_3\left(r_3^2 - r_1^2\right)\frac{M(s)}{P(s)},
\end{aligned} \tag{10}$$

where

$$\begin{aligned}
M(s) &= (1 + s^2 - r_1^2 - \eta_1)(1 + s^2 - r_3^2)\left[r_1\mathrm{sh}(Lr_1) - r_3\mathrm{sh}(Lr_3)\right],\\
P(s) &= \frac{r_1r_3(r_3^2 - r_1^2)\left[r_3(1 + s^2 - r_1^2)\mathrm{ch}(Lr_1)\mathrm{sh}(Lr_3) - r_1(1 + s^2 - r_3^2)\mathrm{ch}(Lr_3)\mathrm{sh}(Lr_1)\right]}{B_0\frac{(\omega\beta)}{s^2+(\omega\beta)^2}},
\end{aligned}$$

and $r_1,\ r_3$ are the roots of the respective characteristic equation for the elastic case [28].

The characteristic equation of Eq. (9) has four real roots due to the fact that the coefficients in (9) satisfy the condition for a positive discriminant for the quadratic equation with a substitution $n = p^2$, e.g.

$$\begin{aligned}
&p^4 + U(s)p^2 + T(s) = 0 \ \Rightarrow\ n^2 + U(s) + T(s) = 0,\\
&U^2(s) - 4T(s) = \left[K_c\left(1 + \lambda^2\right) - s^2\left(1 + c^2\right)\right]^2 - 4s^2\left[c^2s^2 - K_c\left(\lambda^2 + c^2\right)\right] > 0.
\end{aligned}$$

Thus, the four real roots are$p_{1,2} = \pm\sqrt{n_1}$, $p_{3,4} = \pm\sqrt{n_2}$. Since the roots n_1 and n_2 are negative, then all set of roots of the bi-quadratic characteristic equation for Eq. (9) and for any frequency ω are pure imaginary.

Then the fundamental solution of Eq. (9) can be given in a form

$$u_A^c(\xi, s) = D_1(s)\cos(p_1\xi) + D_2(s)\sin(p_1\xi) + D_3(s)\cos(p_3\xi) + D_4(s)\sin(p_3\xi) + \frac{Y(s)}{T(s)}, \tag{11}$$

$$u_B^c(\xi, s) = \frac{1}{K_c}\left(\frac{d^2u_A^c(\xi, s)}{d\xi^2} + \left(K_c - s^2\right)u_A^c(\xi, s) - \frac{\tau^{cr}}{s}\right),$$

where the integration constants $D_1(s)\ i = 1\ldots4$, satisfying the contact conditions (10) are expressed as

$$\begin{aligned}
D_1(s) = {}& \frac{P(s)\,p_1\cos(l_ep_1)\left(Y(s)\,s\,p_3^2 - T(s)\,\tau^{cr}\left(p_3^2 + s^2 + 1 - K_c\right)\right)}{P(s)\,T(s)p_1\,s\,(p_1^2 - p_3^2)}\\
&- \frac{M(s)T(s)\sin(l_ep_1)\,r_1\,r_3\,s\,K_c(r_1^2 - r_3^2)}{P(s)\,T(s)p_1\,s\,(p_1^2 - p_3^2)},\\
D_2(s) = {}& \frac{P(s)\,p_1\sin(l_ep_1)\left(Y(s)\,s\,p_3^2 - T(s)\,\tau^{cr}\left(p_3^2 + s^2 + 1 - K_c\right)\right)}{P(s)\,T(s)p_1\,s\,(p_1^2 - p_3^2)}\\
&+ \frac{M(s)T(s)\cos(l_ep_1)\,r_1\,r_3\,s\,K_c(r_1^2 - r_3^2)}{P(s)\,T(s)p_1\,s\,(p_1^2 - p_3^2)},
\end{aligned}$$

$$D_3(s) = \frac{P(s)\,p_3\cos(l_e p_3)\left(Y(s)\,s\,p_1^2 - T(s)\,\tau^{cr}\,\left(p_1^2+s^2+1-K_c\right)\right)}{P(s)\,T(s)p_1\,s\,(p_1^2-p_3^2)} - \frac{M(s)T(s)\sin(l_e p_3)\,r_1\,r_3\,s\,K_c(r_1^2-r_3^2)}{P(s)\,T(s)p_1\,s\,(p_1^2-p_3^2)},$$

$$D_4(s) = \frac{P(s)\,p_3\sin(l_e p_3)\left(Y(s)\,s\,p_1^2 - T(s)\,\tau^{cr}\,\left(p_1^2+s^2+1-K_c\right)\right)}{P(s)\,T(s)p_1\,s\,(p_1^2-p_3^2)} + \frac{M(s)T(s)\cos(l_e p_3)\,r_1\,r_3\,s\,K_c(r_1^2-r_3^2)}{P(s)\,T(s)p_1\,s\,(p_1^2-p_3^2)}. \tag{12}$$

Then the following solution for the interface shear stress is obtained:

$$\begin{aligned}\tau^I(\xi,s) &= \tau^{cr} - K_c\left(u_A(\xi,s) - u_B(\xi,s)\right)\\ &= \tau^{cr} - K_c\left(u_A(\xi,s) - \frac{1}{K_c}\left(\frac{\partial^2 u_A^c(\xi,s)}{\partial\xi^2} + \left(K_c - s^2\right)u_A^c(\xi,s) - \frac{\tau^{cr}}{s}\right)\right)\\ \Rightarrow \tau^I(\xi,s) &= \tau^{cr} - K_c\left(u_A(\xi,s) - u_B(\xi,s)\right) = \frac{\partial^2 u_A^c(\xi,s)}{\partial\xi^2} - s^2 u_A^c(\xi,s) + \frac{(1+s)}{s}\tau^{cr}.\end{aligned} \tag{13}$$

Following Manolis and Beskos (1987) [35] we will calculate by inverse Laplace transform the original of the shear stress Laplace image. Further, to calculate the debond length at given time interval and the pair of loading characteristics, the special condition for on the value of the interface shear stress has to be satisfied.

Let $[0,T]$ is the time interval, while $K,\ N$ are positive integers and $t_j = \beta\eta_j = \frac{jT}{N},\ j = 0,\ldots,N-1$.

As is underlined in Manolis and Beskos [35] it is assumed, that for $K.N \in [50,\ 5000]$ it should be chosen $b.T \in [5,\ 10]$ in order to have an accurate result (see (13a)). Note, that the proposed procedure is valid for every length of a time interval.

Then $\tau^I(\xi,t_j)$ must be calculated in the discrete set of points $t_j = \beta\eta_j$ and $\xi \in [0,L]$ through formulae

$$\tau^I(\xi,t_j) = \frac{2}{T}\mathrm{e}^{bt_j}\left[-\frac{1}{2}\mathrm{Re}\left(\tilde{\tau}^I(\xi,b)\right) + \mathrm{Re}\left(\sum_{j=0}^{N-1}\left(A_n + iB_n\right)W^{jn}\right)\right], \tag{13a}$$

where

$$A_n = \sum_{k=0}^{K}\mathrm{Re}\tilde{\tau}^I\left(\xi,\left(b + i\,(n+kN)\,\frac{2\pi}{T}\right)\right), \quad B_n = \sum_{k=0}^{K} Im\tilde{\tau}^I\left(\xi,\left(b + i\,(n+kN)\,\frac{2\pi}{T}\right)\right),$$

$$n = 0,\ldots,N, \quad W = \mathrm{e}^{i\frac{2\pi}{N}}.$$

So to find a time dependent shear stress $\tau^I(\xi,t)$ for $t \in [0,T]$ we have to solve the problem in a Laplace domain for all values of the parameter $s_n = b + in\frac{2\pi}{T}\ ,\ n = 0,\ldots,N$. The Mathematica 5.2 program is used to calculate $A_n,\ B_n$, and $\tau^I(\xi,t_j)$. In Sect. 3.1 the small value of the time interval is chosen. The respective figures illustrate the dynamic interface delamination at the initial state.

3.1 Length of a single cohesive debonding

To find a single debond length for cohesive zone, the following assumption on the value of the shear stress is proposed:

If $\tau^I(\xi_1,s) = 0$, where $\xi_1 = l_e - l_c$, then $0 = \tau^{cr} - K_c(u_A(\xi,s) - u_B(\xi,s)) \Rightarrow \tau^{cr} = K_c u_I(\xi,s)$.

We have

$$\tau^I(\xi,s) = \tau^{cr} - K_c\left(u_A\left(\left(l_e - l_c\right),s\right) - u_B\left(\left(l_e - l_c\right),s\right)\right). \tag{14}$$

The equation for finding the single debond cohesive length regards

$$\frac{\partial^2 u_A^c(\xi,s)}{\partial\xi^2} - s^2 u_A^c(\xi,s) + \frac{(1+s)}{s}\tau^{cr} = 0. \tag{15}$$

The parametric analysis on the influence of material and geometric characteristics as well as the frequency of the applied loading on the behaviour of the τ^I , l_e, and l_c along the interface will be illustrated by figures in Sect. 4.

3.2 Cohesive debond length of the interface zone

The single debond length l_c which gives the magnitude of the cohesive cracking along the interface can be calculated from Eq. (15) under assumption that the shear stress reaches its zero value $\tau^I(l_c, t_j) = 0$. Using the inverse Laplace transform the value of the corresponding single elastic debond length is taken into account. When calculating the value of a single cohesive debond length the following criterion is proposed:

$$l_e + l_c \leq L, \tag{16}$$

where L is the non-dimensional value of the length of the structure, respectively of the interface.

The parametric analysis of the influence of material and geometric characteristics as well as the frequency of the applied loading on the behaviour of τ^I and l_e, l_c along the interface will be illustrated by figures in Sect. 4. The single debond length corresponds to a given value of the amplitude with given value of a time.

4 Results and discussion

4.1 Numerical data

Starting numerical calculations for cohesive debond lengths the authors will use non dimensional geometries and material properties for bi-material structures considered in [34], where the elastic debond lengths are already calculated. To simplify the calculations for inverse Laplace transform the time interval $T = [0,\ 8\,]$ s is taken as in [34]. Note that these calculations for the originals can be performed for every value of the time interval. The inertia forces from the already debonded along the interface parts of the first plate are neglected from the simplicity reason in the case of thick first plate. Further the thin first plate will be considered. Under such an assumption the inertia forces don't play significant role due to their small values inertial characteristics.

Let us consider two elastic plates A and B with finite lengths $2L = 1.2\,\text{m}$ and thickness $2h_A = 0.2\,\text{m},\ 2\,h_B = 1\,\text{m}$, under the dynamic loading $A_0 \sin(\omega t)$ for time interval $T \in [0,\ 8\ ]$ s, where $A_0 \in [1,\ 6] \times 10^9\,\text{Nm}^{-2},\ \omega \in [1436.07,\ 17232.8]\,\text{s}^{-1}$ are the amplitude and the angle frequency, respectively. Further the non-dimensional frequency $\Omega = kL = \frac{\omega}{C}L = \frac{2\pi}{\lambda}L$ and non dimensional geometry and material characteristics will be used. Here k, ω, C, λ denote the wave number, angle frequency, velocity of the wave propagating $C = C_A = \sqrt{E_A/\rho_A}$ in layer A, and the length of the wave, respectively.

The material properties (a polyacrilate thermoplastic glue) of the interface are presented by the shear modulus is $G^I = 800$ MPa, the critical shear stress $\tau^I = \tau^{cr} = 18\,\text{MPa}$ and with the softening modulus $K_c = 20\,MPa$, where this value of the softening modulus are taken to be fictitious. The value of the softening modulus is chosen to illustrate the arising of the single cohesive debond length at the abovementioned criterion (15).

The following mechanical, non-dimensional parameters and frequencies for the bi-material structure are shown on Table 1, Table 2, and Table 3.

Table 1 Mechanical characteristics.

Material	E [GPa]	ρ [kg/m^3]
Steel $(440C)$	200	7650
Aluminium (Al)	60	2700
Cermet (85% Al_2O_3 +15% Al)	294	3960

As it was underlined in [34], there exist two important limit values of the frequency: Ω_1 – the frequency when the elastic-brittle delamination process begins and Ω_2 – when the full elastic brittle delamination occurs, see Table 3. So, the frequency interval $\Omega \in [0.1,\ 1.2]$ should be considered.

Table 2 Non-dimensional parameters.

Type of bi-material structure	α	β	η_1	μ	ς	L
Cermet (85% Al_2O_3 +15% Al)/Al	6.641	0.001	4.899	1.467	0.2	0.09
Cermet (85% Al_2O_3 + 15% Al)/Steel $(440C)$	6.641	0.001	1.47	0.518	0.2	0.09

Table 3 Loading frequencies Ω.

Type of bi-material structure	Ω_1	Ω_2
Cermet (85% $Al_2O_3 + 15\%$Al)/Al	1.02	less than 0.68
Cermet (85% $Al_2O_3 + 15\%$ Al)/Steel $(440C)$	1.01	less than 0.97

Substituting the values of the above parameters in equations for $\tau^I(\xi, t_j)$ we obtain an elastic-brittle solution, describing in [34]:

- The dependence of the debond length l_e on the frequency of the applied dynamic load with fixed amplitude $B_0 = A_0 a_0/(E_A G)^{1/2} = 0.150584$, where $A_0 = 4 \times 10^9$ N/m^2 and $a_0 = [2h_A/(h_A + h_B)]$.
- The dependence of the shear stress $\tau^I(\xi, t_j)$ versus ξ at dynamic load with fixed frequency $\Omega = 1$ for the different bi-material structures.
- The dependence of the single debond length l_e on non-dimensional amplitude B_0 of the applied dynamic load with fixed frequency $\Omega = 1$.

Following [34] all parameters in the next figures are taken to be non-dimensional ones.

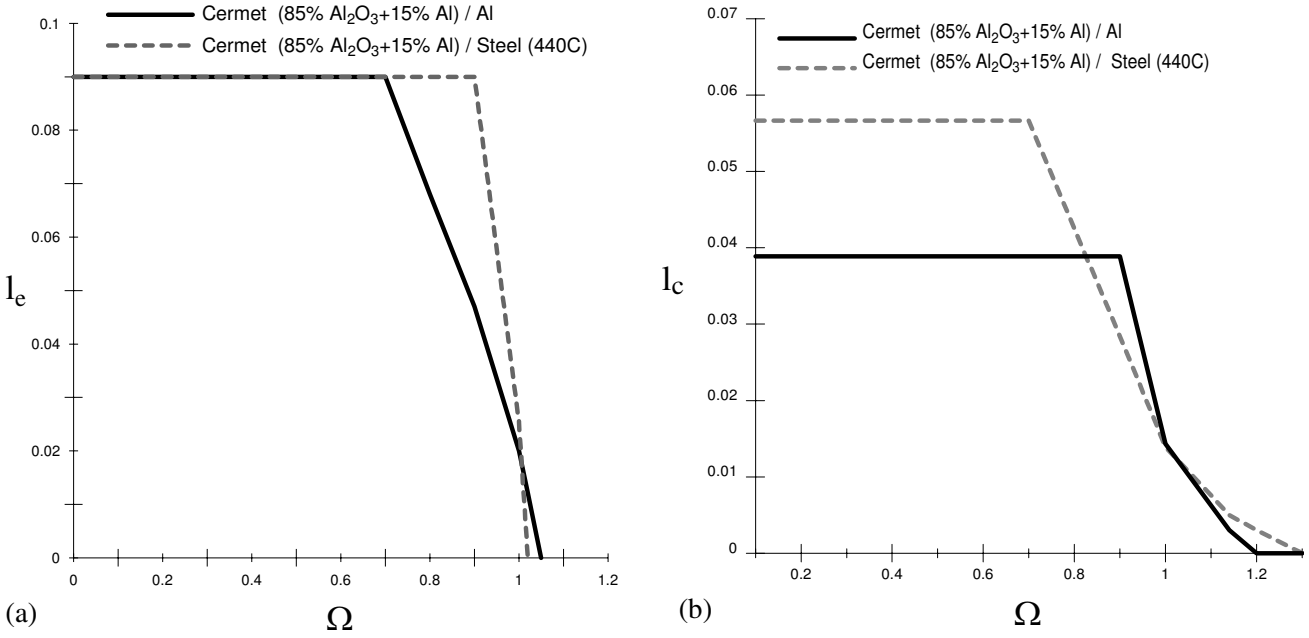

Fig. 3 Dependence of the debond lengths l_e and l_c on the frequency Ω of the applied load at fixed value of the amplitude $B_0 = A_0 a_0/(E_A G)^{1/2} = 0.150584$ for the different bi-material structures.

By the aid of the obtained single elastic-brittle length and the same loading condition Eq. (15) is resolved to obtain the corresponding single cohesive debond length. Figs. 3 show the dependences of the single debond lengths l_e and l_c on the non-dimensional frequency Ω at fixed value of the amplitude $B_0 \in [0.037647,\ 0.225876]$, i.e. l_e and l_c decreases with increasing of the frequency Ω. The full delamination occurs at lower frequencies Ω_2, i.e. $\frac{L}{\lambda} \in [0.016,\ 0.193]$. As expected, the single cohesive debond length are much smaller comparing with values of the respective single elastic debond length.

The behaviour of the shear stress $\tau^I(\xi, t)$on$\xi \in [l_e,\ L]$ at time-harmonic dynamic load with frequency $\Omega = 1$ for two different bi-material structure is shown in Fig. 4.

This figure clearly evidences the influence of ξ to the shear stress for the given value of frequency $\Omega = 1$. For the different bi-material structure at constant amplitude of the applied mechanical time harmonic load $B_0 = 0.150584$, the single elastic and cohesive debond lengths l_e and l_c have the following values:

- $l_e = 0.03027$ and $l_c = 0.0115$ Cermet (85% $Al_2O_3 + 15\%$ Al)/Al,
- $l_e = 0.0415$ and $l_c = 0.0176$ Cermet (85% $Al_2O_3 + 15\%$ Al)/Steel $(440C)$.

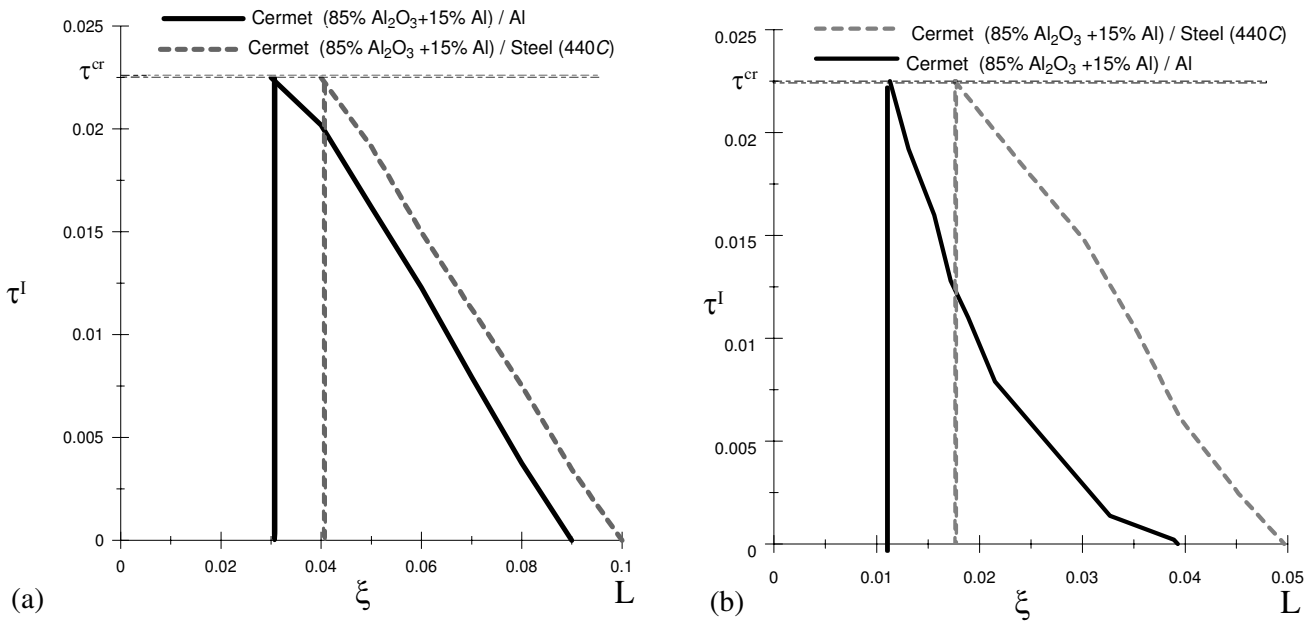

Fig. 4 Distribution of the shear stress versus ξ at dynamic load with frequency $\Omega = 1$ for the different bi-material structures.

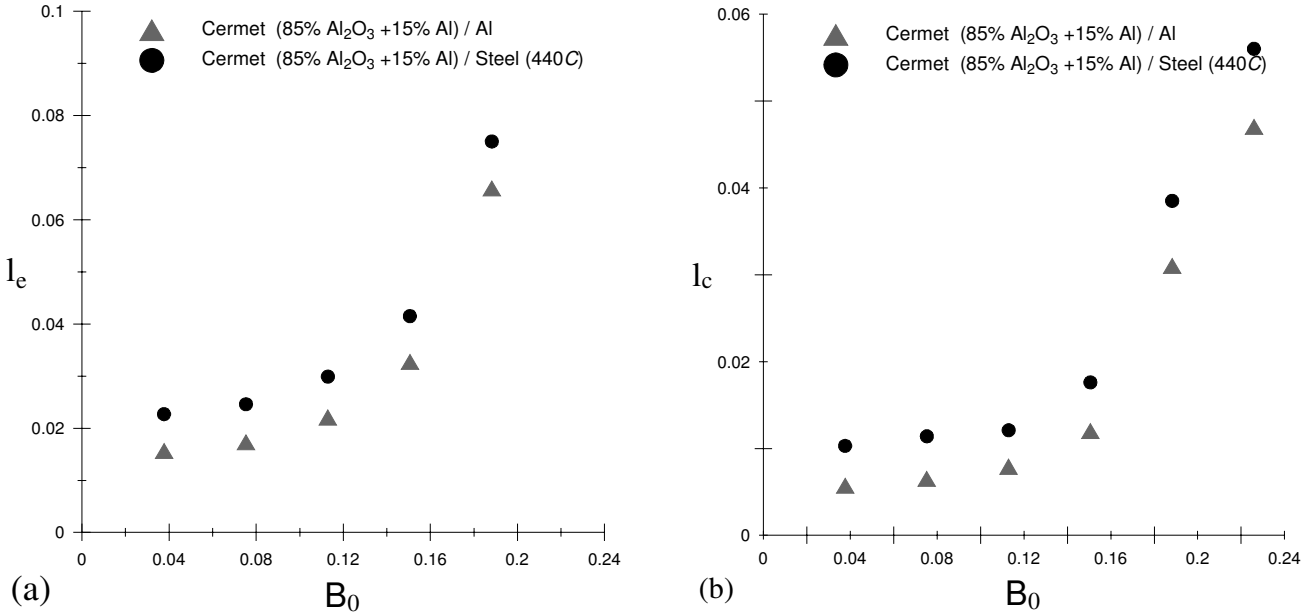

Fig. 5 Dependence of the debond lengths l_e and l_c on non-dimensional amplitudes of the applied dynamic B_0 at non-dimensional frequency $\Omega = 1$ for the different bi-material structures and time interval $t \in [0\,,\ 8]$ s.

The interface shear stress reaches to the critical shear stress and $\tau^I(l_e) = \tau^{cr} = 0.0225$. When the single debond length l_e for the different bi-material constructions tends towards L, the full delamination process occurs.

Fig. 5 shows that the single elastic and cohesive debond lengths (l_e and l_c) strongly depend on the amplitude of the applied dynamic load, i.e. both increases with increase of the load amplitude and this dependence is sensitive to the material properties of the bi-material structure. It can be seen, that for a given interval of amplitude of applied load, the material properties of the second plate play an important role. If Aluminium is used for the second plate, the value of single debond lengths are smaller and arises earlier, comparing with Steel ($440\,C$) plate ($t \in [0\,,\ 8]$ s).

Fig. 6 presents the parametric analysis of the single debond lengths l_e and l_c from the geometric ratio ς and load frequency. It is shown, that the single elastic l_e and cohesive l_c debond lengths strongly depend from the geometric ratio ς

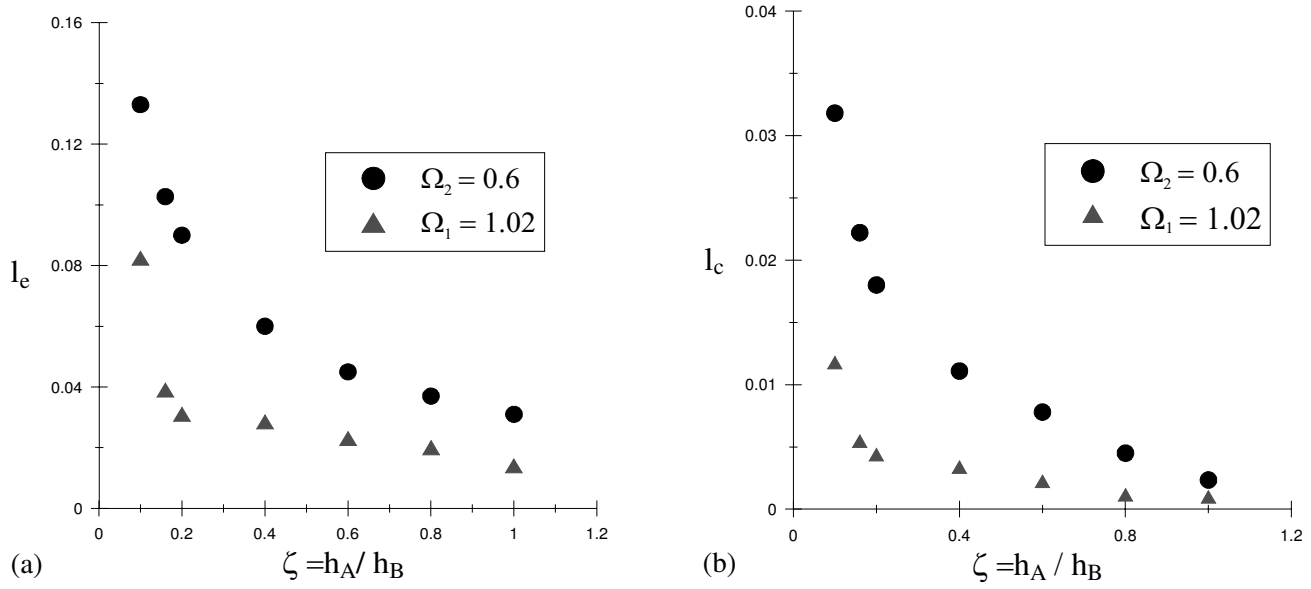

Fig. 6 Dependence of the debond lengths l_e and l_c from ς for two values of frequency $\Omega = 0.6; 1.02$ and time $t \in [0\,,\ 8]$ s for Cermet (85% $Al_2O_3 + 15\%$ Al)/Al structure.

and from the frequency of the applied dynamic load, i.e. both l_e and l_c decrease with increasing of the load frequency or time $t \in [0,\ 8]$ s along the axis ς.

The delamination process begins when the frequency Ω_2 is less the 0.68 and the full delamination occurs for frequency $\Omega_1 = 1.02$. The last case leads to a full degradation of the structures.

5 Conclusion

In this paper a mathematical modeling of dynamic stress behaviour and an cohesive interface delamination of bi-material plates subjected to sinusoidal dynamic loading with the normal pre-crack of the first plate reaching the interface and debonded along the interface with a single debond elastic-brittle length was investigated. To study the problem, the shear lag model was adopted and applied to dynamic problems of bi-material structure, assuming the cohesive behaviour of the interface material accompanied by an the elastic-brittle debonding.

The inverse Laplace transform was used to obtain the single cohesive debond length along the interface of bi-material structure. The parametric analyses of the single elastic and cohesive debond lengths from amplitude of loading and geometric ration ς are illustrated by figures and discussed.

Acknowledgements Bi-lateral project of BAS/PAS "New composite materials, homogenization and macroscopic behaviour of structural elements" (2009–2011) and European social fund, operational program "Human resources development", Grant No. BG051PO001/-07/3.3-02-55/17.06.2008.

References

[1] P. J. Dowling and B. A. Burgan, Shear Lag in Steel and Composite Structures. In: Composite Steel Structures. Advances, Design and Construction, edited by R. Narayanan (Spon Press, London, 1990) pp. 1–23.
[2] L. H. Cox, The elasticity and strength of paper and other fibrous materials, Br. J. Appl. Phys. **3**, 72–79 (1952).
[3] J. M. Hedgepeth, Stress Concentrations in Filamentary Structures. NASA TN D-882 (Langley Research Center, Langley, 1961).
[4] S. V. Kulkarni, B. W. Rosen, and C. Zweben, Load concentration factors for circular holes in composite laminates, J. Comput. Math. **7**, 387–393 (1973).
[5] J. A. Nairn, Fracture mechanics of unidirectional composites using the shear-lag model I: Theory, J. Comput. Math. **22**(6), 561–588 (1988).
[6] J. A. Nairn, Fracture mechanics of unidirectional composites using the shear-lag model II: Experiment, J. Comput. Math. **22**(6), 589–600 (1988).
[7] J. A. Nairn, S. Liu, and H. Chen, Wedgewood longitudinal splitting in epoxy and k-polymer composites: shear-lag analysis including the effect of fiber bridging, J. Comput. Math. **25**, 1086–1107 (1990).

[8] S. L. Phoenix and I. J. Beyerlein, Statistical Strength Theory for Fibrous Composite Materials, Chap. 1.19 in Vol. 1, edited by T.-W. Chou, of Comprehensive Composite Materials series, edited by A. Kelly and C. Zweben (Pergamon-Elsevier Science, Amsterdam, 2000) pp. 559–639.
[9] J. Lemaitre, R. Desmorat, M. P. Vidonne, and P. Zhang, Reinitiation of a crack reaching an interface, Int. J. Fract. **80**, 257–276 (1996).
[10] T. S. Cook and F. Erdogan, Stresses in bonded materials with a crack going through the interface, Int. J. Eng. Sci. **11**, 745–766 (1973).
[11] A. Rizk and F. Erdogan, Cracking of coated materials under transient thermal stresses, J. Therm. Stresses **12**, 125–168, (1989).
[12] J. W. Hutchinson and Z. Suo, Mixed mode cracking in layered materials, Adv. Appl. Mech. **29**, 62–191 (1992).
[13] J. Ivanova, V. Valeva, and Z. Mroz, Mechanical modelling of the delamination of bi-material plate structure, J. Theor. Appl. Mech. (Sofia) **36**(4), 39–54 (2006).
[14] G. Nikolova, J. Ivanova, V. Valeva, and Z. Mroz, Mechanical and thermal loading of two-plate structure, C.R. Acad. Bulg. Sci. **60**(7), 735–745 (2007).
[15] G. Nikolova and J. Ivanova, Cracked Biomaterial Plates Under Thermomechanical Loading, Proceedings Fractography of Advanced Ceramics III, in Key Material series, Vol. 413 (Trans Tech Publications Ltd., Dürnten, 2009) pp. 406–413.
[16] G. Nikolova, Thermo-Mechanical Behaviour of Thin Graded Layered Structures – PhD Thesis, (Institute of Mechanics, BAS, Sofia, 2008).
[17] G. M. Song, W. G. Sloof, Y. T. Pei, and J. Th. M. De Hosson, Interface behaviour of zinc coating on steel: Experiments and finite element calculations, Surf. Coat. Technol. **201**, 4311–4316, (2006).
[18] J. L. Beuth Jr., Cracking of thin films in thin bonded films in residual tension, Int. J. Solids Struct. **29**(13), 1567–1675 (1992).
[19] J. W. Hutchinson and Z. Suo, Mixed mode cracking in layered materials, Adv. Appl. Mech. **28**, 63–189 (1991).
[20] J. L. Beuth and N. W. Klingbeil, Cracking of thin films bonded to elastic-plastic substrates, J. Mech. Phys. Solids **44**(9), 1411–1428 (1996).
[21] Y. G. Wei and J. W. Hutchinson, Nonlinear delamination mechanics for thin films, J. Mech. Phys. Solids **45**(7), 1137–1159 (1997).
[22] H. C. Choi and K. S. Kim, Analysis of the spontaneous interfacial decohesion of a thin surface film, J. Mech. Phys. Solids **40**(1), 75–103 (1992).
[23] B. Chen and T.-W. Chou, Local elastodynamic stresses in the unit cell of a woven fabric composite, Arch. Appl. Mech. **70**, 423–442 (2000).
[24] B. Chen and T.-W. Chou, The propagation of one-dimensional transient elastic waves in woven-fabric composites, Comp. Sci. Technol. **58**, 1385–1396 (1998).
[25] Y. L. Li, C. Ruiz, and J. Harding, Stress wave propagation in hybrid composite materials, J. Reinf. Plast. Compos. **10**(4), 400–422 (1991).
[26] G. J. Barenblatt, The formulation of equilibrium cracks during brittle fracture. General ideas and Hypothesis. Axisymmetric cracks, Priklud. Mat. Mekh. **23**, 434–444 (1957).
[27] D. S. Dugdale, Yielding of steel containing slits, J. Mech. Phys. Solids **8**, 100–104 (1960).
[28] A. Hilleborg, M. Modeer, and P. E. Peterson, Analysis of crack formation and crack growth in concrete by means of fracture mechanics and finite elements, Cement Concr. Res. **6**, 773–782 (1976).
[29] J. H. Rose, J. Ferrante, and J. R. Smith, Universal features of bonding in metals, Phys. Rev. B **28**, 1835–1845 (1982).
[30] A. Needleman, A continuum model for void nucleation by inclusiom debonding, Trans. ASME J. Appl. Mech. **54**, 525–531 (1987).
[31] V. Twergaard, Effect of fibre debonding in a whisker-reinforced metal, Mater. Sci. Eng. A **125**, 203–213 (1990).
[32] V. Twergaard and J. W. Hutchinson, The relation between crack growth resistance and fracture process parameters in elastic-plastic solids, J. Mech. Phys. Solids **40**, 1377–1397 (1992).
[33] X. P. Xu and A. Needleman, Void nucleation by inclusion debonding in a crystal matrix, Model. Simul. Mater. Sci. Eng. **1**, 111–132 (1993).
[34] J. Ivanova, G. Nikolova, and B. Gambin, Interface delamination of bi-material structure under dynamic time harmonic loading, Z. Angew. Math. Mech. **91**, 146–154 (2011).
[35] G. Manolis and D. Beskos, Boundary Element Methods in Elastodynamics (Boston, Allen and Unwin, Inc. London, Sydney, 1987).

